Superconductivity, Mott–Hubbard states, and molecular orbital order in intercalated fullerides

2003 J. Phys.: Condens. Matter 15 R495

(http://iopscience.iop.org/0953-8984/15/13/202)

INSTITUTE OF PHYSICS PUBLISHING JOURNAL OF PHYSICS: CONDENSED MATTER

J. Phys.: Condens. Matter **15** (2003) R495–R519 PII: S0953-8984(03)18273-2

TOPICAL REVIEW

Superconductivity, Mott–Hubbard states, and molecular orbital order in intercalated fullerides

Y Iwasa[1,2] **and T Takenobu**[1,2]

[1] Institute for Materials Research, Tohoku University, 2-1-1 Katahira, Aoba-ku, Sendai 980-8577, Japan
[2] CREST, Japan Science and Technology Corporation, Kawaguchi 332-0012, Japan

Received 14 January 2003
Published 24 March 2003
Online at stacks.iop.org/JPhysCM/15/R495

Abstract

This article reviews the current status of chemically doped fullerene superconductors and related compounds, with particular focus on Mott–Hubbard states and the role of molecular orbital degeneracy. Alkaline-earth metal fullerides produce superconductors of several kinds, all of which have states with higher valence than $(C_{60})^{6-}$, where the second lowest unoccupied molecular orbital (the LUMO + 1 state) is filled. Alkali-metal-doped fullerides, on the other hand, afford superconductors only at the stoichiometry A_3C_{60} (A denotes alkali metal) and in basically fcc structures. The metallicity and superconductivity of A_3C_{60} compounds are destroyed either by reduction of the crystal symmetry or by change in the valence of C_{60}. This difference is attributed to the narrower bandwidth in the A_3C_{60} system, causing electronic instability in Jahn–Teller insulators and Mott–Hubbard insulators. The latter metal–insulator transition is driven by intercalation of ammonia molecules into A_3C_{60}-type superconductors. Furthermore, the triple degeneracy of the LUMO state of C_{60} plays a crucial role in the metal–insulator transition and in controlling the magnetic structures of insulating states, possibly providing novel properties of degenerate orbitals. The goal of this article is to establish a unifying picture of fullerene intercalation compounds, and to clarify the underlying physics: competing energy scales and orbital properties of molecule-based systems.

(Some figures in this article are in colour only in the electronic version)

Contents

1. Introduction: the current status of fullerene superconductors

The development of the Krätchmer–Huffman method of mass production of fullerene molecules [1] in 1990 motivated solid-state fullerene research, as a result of which the superconductivity of A_3C_{60} fullerides was discovered [2, 3]. (Here, A denotes alkali metal.) Subsequent to the maximum critical temperature (T_c) of 33 K at ambient pressure being achieved in 1991 [4], C_3C_{60} was found to be superconducting only under high pressure and to show a broad onset at 40 K [5]. These transition temperatures are the second highest among noncuprate superconductors [6]. Figure 1 shows a C_{60} molecule and its three molecular orbitals crossing the Fermi energy. The highest occupied molecular orbital (HOMO) is fivefold degenerate, having h_u symmetry, while the lowest unoccupied molecular orbital (LUMO) and the LUMO + 1 states are both triply degenerate, with t_{1u} and t_{1g} symmetry, respectively. To date, the two LUMO levels have been accessed either by chemical doping or the field-effect-transistor technique [7]. Among the approaches tried, chemical intercalation of C_{60} with metals has produced a particularly rich variety of conducting compounds with carriers introduced in the t_{1u} and t_{1g} bands. It is well established that bulk superconductivity is observed both in t_{1u} and t_{1g} bands. The highest values of T_c for the t_{1g} and t_{1u} states are 8 and 33 K (40 K at high pressure), respectively.

Table 1 summarizes the characteristics of fullerene superconductors, which are chemically and structurally identified. Not only alkali metals but also alkaline-earth and rare-earth metals are known to afford C_{60}-based superconductors. For providing a simpler view of fullerene superconductivity, the nominal electron count n per C_{60} molecule (the molecular valence), which is calculated from the ionic crystal model, is quite useful. For example, in the case of K_3C_{60} [3], the value of n is 3. In the case of Ba_4C_{60} [24], n is estimated to be 8, since Ba is nominally divalent. Because the two LUMOs (t_{1u} and t_{1g} states) of C_{60} are both triply degenerate (figure 1), the issue of intercalation of C_{60} with metals is regarded as that of filling two triply degenerate orbitals with electrons. When the valence n is smaller than 6, only the t_{1u} state is filled with electrons. When n exceeds 6, the LUMO is fully occupied and the t_{1g} state is filled. The highest n obtained so far is 12, as seen in Ba_6C_{60} and Sr_6C_{60} [22, 29].

From the above point of view, alkali-doped C_{60} superconductors are classified into one group, namely, the trivalent ($n = 3$) system, despite the variety and complexity of the materials. Several ammonia-containing compounds, which will be discussed in the following sections, are also included in the $n = 3$ group, since ammonia molecules are incorporated in a neutral state. Generally speaking, alkaline-earth and rare-earth compounds yield compounds with higher

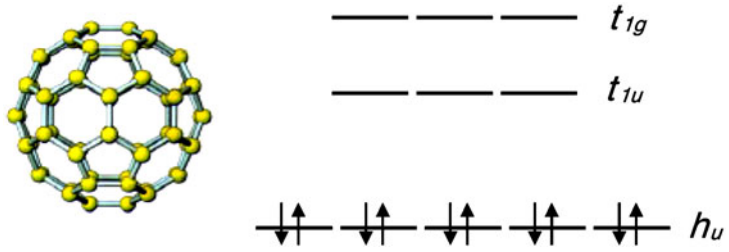

Figure 1. The molecular structure and electronic energy levels of neutral C_{60} around the Fermi energy.

Table 1. Chemically and structurally identified fullerene superconductors.

Compounds	Structure	Lattice parameters (Å)	T_c (K)	References
		Alkali-metal-doped C_{60}		
Li_3CsC_{60}	fcc	$a = 14.080$	10.5	[8]
Na_2KC_{60}	fcc	$a = 14.122$	2.5	[9, 10]
Na_2RbC_{60}	fcc	$a = 14.092$	3.5	[9, 10]
Na_2CsC_{60}	fcc	$a = 14.126$	12	[9, 10]
K_3C_{60}	fcc	$a = 14.240$	19	[3, 10]
$K_xRb_{3-x}C_{60}$ $(0 < x < 3)$	fcc	$a = 14.24$–14.29	19–29	[11]
K_2CsC_{60}	fcc	$a = 14.292$	24	[11]
Rb_3C_{60}	fcc	$a = 14.384$	29	[12]
Rb_2CsC_{60}	fcc	$a = 14.431$	31	[11]
$RbCs_2C_{60}$	fcc	$a = 14.555$	33	[4]
Cs_3C_{60}	bct	$a = 12.06$, $c = 11.43$	40 (high P)	[5]
$(NH_3)_4Na_2CsC_{60}$	fcc	$a = 14.473$	30	[13]
$(NH_3)_xNaK_2C_{60}$ $(0.5 < x < 1)$	fcc	$a = 14.35$–14.40	8–13	[14]
$(NH_3)_xNaRb_2C_{60}$ $(0.5 < x < 1)$	fcc	$a = 14.50$–14.53	8.5–17	[14]
$(NH_3)K_3C_{60}$	bco	$a = 14.971$, $b = 14.895$, $c = 13.678$	28 (high P), AFI ($P = 1$ bar)	[15], [16]
$(NH_3)_xK_3C_{60}$ $(0 < x < 1)$	fcc	$a = 14.32$	8.5	[17]
$Na_xN_yC_{60}$	fcc	$a = 14.204$	12	[18]
Na_xNyC_{60}	fcc	$a = 14.356$	15	[19]
		Alkaline-earth-metal-doped C_{60}		
Ca_5C_{60}	sc	$a = 14.01$	8.4	[20]
Sr_4C_{60}	bco		4	[21]
Ba_4C_{60}	bco	$a = 11.610$, $b = 11.234$, $c = 10.882$	6.7	[22, 23] [24]
$K_3Ba_3C_{60}$	bcc	$a = 11.245$	5.6	[25]
$Rb_3Ba_3C_{60}$	bcc	$a = 11.338$	2.0	[26]
$K_2Ba_4C_{60}$	bcc	$a = 11.212$	3.6	Present result
		Rare-earth-metal-doped C_{60}		
$Yb_{2.75}C_{60}$	Orthorhombic	$a = 27.87$, $b = 27.98$, $c = 27.87$	6	[27]
$Sm_{2.75}C_{60}$	Orthorhombic	$a = 28.17$, $b = 28.07$, $c = 28.27$	8	[28]

valence. The highest valence that has been identified for a superconducting phase is $n = 10$, for Ca_5C_{60} [20]. Combination of alkali and alkaline-earth metals produces new compounds with unique valence states. For instance, the valence of $K_3Ba_3C_{60}$ [25] is estimated to be $n = 9$, which had not been achieved in simple binary phases. Yb- or Sm-doped compounds also yield superconductors. According to x-ray photoemission spectroscopy, the Yb ion is divalent in the $Yb_{2.75}C_{60}$ superconducting phase [27, 30]. Thus, the valence n of C_{60} is estimated to be 5.5.

A relation between T_c and the formal valence of C_{60} is presented in figure 2. First, it should be pointed out that doping with alkali metals produces only trivalent superconductors with the fcc structure. The highest T_c (33 K) at ambient pressure among the chemical methods is obtained in the alkali-metal-doped compound. Generally, alkaline-earth and rare-earth metals produce compounds with higher valence states. In particular, intercalation of alkaline-

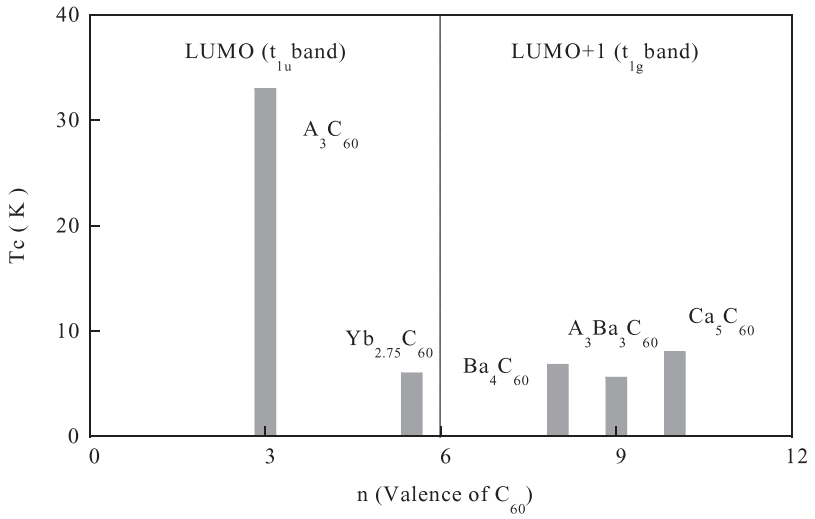

Figure 2. The relation between T_c and the formal valence of C_{60}, where the highest T_c for each group is presented. The formal valence is calculated assuming monovalent alkali ions and divalent alkaline-earth and rare-earth ions. For $0 < n < 6$, the t_{1u} band is partially filled, while the t_{1g} band is partially filled for $6 < n < 12$.

earth metal yields superconductors with various valences and crystal structures. However, T_c for these high-valence materials is substantially lower than those of alkali-metal-doped compounds.

One of the goals of this article is to review the properties of several superconducting compounds with the t_{1g} conduction band, which is achieved only by intercalation of alkaline-earth metals. A number of review articles already published have not paid much attention to the t_{1g} system [31–34], because of the relatively low values of T_c and the poor characterization as compared to alkali-metal-doped C_{60} systems. However, since the chemical and structural criteria for the occurrence of superconductivity in the t_{1g} band differ considerably from those for the t_{1u} system, comparison between t_{1g} and t_{1u} systems is helpful for obtaining a comprehensive understanding. Thus the first aim of this article is to construct a unifying picture of the electronic states of fullerene superconductors occurring in t_{1g} and t_{1u} bands.

Another important characteristic of fullerene superconductors is the empirical relation between T_c and the interfullerene separation in the trivalent fcc series of superconductors, which is displayed in figure 3. The increase of T_c with the unit-cell volume (or interfullerene separation) was established early in 1991, and has been believed to be strong evidence for the BCS mechanism of fullerene superconductivity, because the mechanism predicts that T_c is controlled by the density of states at the Fermi energy $N(\varepsilon_F)$, and that enhancement of T_c or $N(\varepsilon_F)$ is achieved when the interfullerene transfer energy is reduced by increasing the separation. There have been a number of efforts investigating the effect of pushing the interfullerene separation to a larger magnitude. For instance, for the $Cs_xRb_{3-x}C_{60}$ system it has been shown that a maximum of T_c in the fcc structure is reached at $x = 2$, and that T_c then starts to decrease with increasing separation [35]. Another approach is to intercalate neutral molecules into the A_3C_{60} lattice so that the interfullerene spacing is increased while the valence of C_{60} is kept unchanged. In particular, intercalation of neutral ammonia molecules has been extensively investigated and a variety of compounds have been reported on. The highest T_c achieved taking this direction is 29 K for $(NH_3)_4Na_2CsC_{60}$ [13]. However, the ammoniation

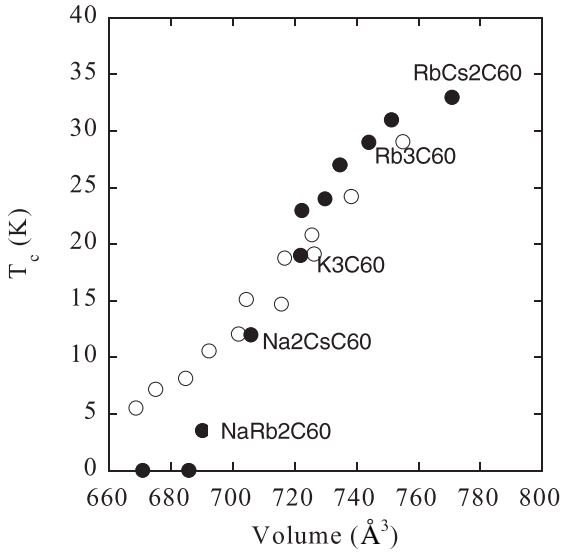

Figure 3. A plot of T_c versus volume/molecule for alkali-metal-doped C_{60} superconductors in the trivalent state ($n = 3$). Filled and open circles are data points at ambient and high pressures, respectively.

technique has revealed a new aspect of fullerene intercalation compounds: the Mott–Hubbard transition and the correlation between the orientation/orbital order of C_{60} molecules and the magnetic structure.

The electron correlation effect has not been apparent in trivalent fullerides, particularly when one pays attention only to superconductors. On the other hands, the importance of electron correlation was indicated experimentally early in 1992, by Auger electron spectroscopy of C_{60} [36]. Researchers found that the on-ball Coulomb energy U is more than 1 eV, which is considerably larger than the bandwidth of typical fullerites. In fact, the electronic ground state of monovalent fullerides (A_1C_{60} polymer) was found to be a spin density wave (SDW) state, indicating that the electron correlation effect does play a crucial role [37]. In the trivalent superconducting materials A_3C_{60}, however, Coulomb interaction or electron correlation has been believed to impose only a minor energy scaling, since the band picture and the BCS scheme were very successful. The first evidence for an electron correlation effect in the vicinity of trivalent superconductors was obtained in 1996 for one of the ammoniated trivalent fullerides, $(NH_3)K_3C_{60}$ [38, 39]. This compound, first synthesized by Rosseinsky and co-workers in 1994 [15], does not superconduct, despite an interfullerene spacing comparable with that of the Rb_2CsC_{60} superconductor with $T_c = 31$ K. The crystal structure of $(NH_3)K_3C_{60}$ is very close to fcc, but has a slight orthorhombic distortion. Electron spin resonance (ESR) studies [38, 39], followed by muon spin rotation (μSR) [40], high-field ESR [41], and nuclear magnetic resonance (NMR) investigations [42], provided unambiguous evidence for an antiferromagnetic insulating ground state for this compound. In other words, the superconductivity of K_3C_{60} is destroyed by insertion of neutral molecules and replaced by an antiferromagnetic state. The most important point relating to this phenomenon is that the transition between the superconductor and the antiferromagnetic insulator is induced by the lattice symmetry, since there remains an orbital degree of freedom in C_{60} compounds with nearly cubic structure [42]. This provided a first example of the orbital degree of freedom

playing an important role in molecule-based materials. The second goal of this article is to review the status of the metal–insulator transition and the effect of orbital degeneracy in trivalent fullerides.

In section 2, the synthesis, structure, and properties of t_{1g} superconductors are presented. In section 3, the electronic properties of compounds with t_{1u} states—particularly, breakdown of the band picture caused by Jahn–Teller instability—is addressed. Section 5 gives a comparative argument regarding properties of t_{1u} and t_{1g} states. In section 4, the Mott–Hubbard transition in ammoniated alkali fullerides is discussed. Section 6 shows that the molecular orientation/orbital order is closely correlated with the magnetic structure in the antiferromagnetic state. Finally, in section 7, a brief summary and perspectives will be given.

2. Barium-doped superconductors in t_{1g} states

Kortan and co-workers [20] discovered, in 1992, superconducting materials in the t_{1g} state, through intercalation with alkaline-earth metals (Ca, Sr, and Ba). They first reported the superconductivity of Ca_5C_{60}, with $T_c = 8$ K. A preliminary structural study suggested that the superconducting phase is fcc-derived simple cubic, but the detailed structure of this phase remains to be established. They subsequently reported the superconductivity of Ba_6C_{60} and Sr_6C_{60} [21, 22]. Later, careful experimental examinations proved that the true superconducting phase is body-centred orthorhombic (bco) Ae_4C_{60}. Here Ae denotes Ba or Sr. Baenitz *et al* [23] were the first to show, in 1995, that the superconducting phase of Ba-doped C_{60} could be orthorhombic. However, since their sample contained the orthorhombic phase as a minority phase, the phase identification was not necessarily conclusive. In 1999, synthesis of single-phase Ba_4C_{60} presented unambiguous evidence for the superconductivity of the orthorhombic Ba_4C_{60} phase [24]. Ba_4C_{60} is the first fully identified noncubic superconductor without a fcc-like arrangement of C_{60} molecules. The crystal structure of Ba_4C_{60} is displayed in figure 4. The structure is similar to the body-centred tetragonal structure of K_4C_{60} and Rb_4C_{60} [43], in which the orientation of the C_{60} molecule is disordered. In contrast, the orientation of the molecule is fully ordered in Ba_4C_{60}, resulting in the space group $Immm$. This structure is identical to that of Cs_4C_{60}, where the increased metal–fullerene interaction due to the large ionic radius causes the full orientational ordering [44]. Although the ionic radius of Ba^{2+} is almost identical to that of K^+, the larger Madelung energy due to the larger ionicity induces the contraction of the lattice parameter and, consequently, the full orientational ordering.

The left-hand panel of figure 5 shows the Raman spectra of pristine and Ba-doped C_{60} compounds [29]. The strongest peak at around 1400 cm^{-1} is assigned as a tangential mode, $A_g(2)$, of C_{60} and is known to be a sensitive probe for the charge transfer to the C_{60} molecule. In the case of alkali metal doping, where full charge transfer is achieved, the Raman shift shows a downshift at a rate of $\sim$7 cm^{-1}/charge [45]. The relation between the Raman shift of the $A_g(2)$ mode and the formal valence is plotted in the right-hand panel of figure 5. The experimental result shows that the Raman shift of Ba_3C_{60} is almost identical to that of K_6C_{60}, and increase of the Ba concentration causes a downshift of the $A_g(2)$ mode at approximately the same rate as in the case of alkali metal doping. This result indicates that the charge transfer from Ba to C_{60} is also nearly complete (in the first-order approximation). In other words, Ba_3C_{60}, Ba_4C_{60}, and Ba_6C_{60} should be close to hexavalent, octavalent, and dodecavalent, respectively. Thus Ba_4C_{60} should have a partially filled t_{1g} band, while Ba_3C_{60} and Ba_6C_{60} have full t_{1u} and t_{1g} bands, respectively.

Mixing of alkaline-earth metals and alkali metals produces a new valence state. An example is provided by $A_3Ba_3C_{60}$ (A = K, Rb, and Cs), which produces a nonavalent state $(C_{60})^{9-}$ according to simple electron counting [25, 26]. The nominal nonavalent state has not

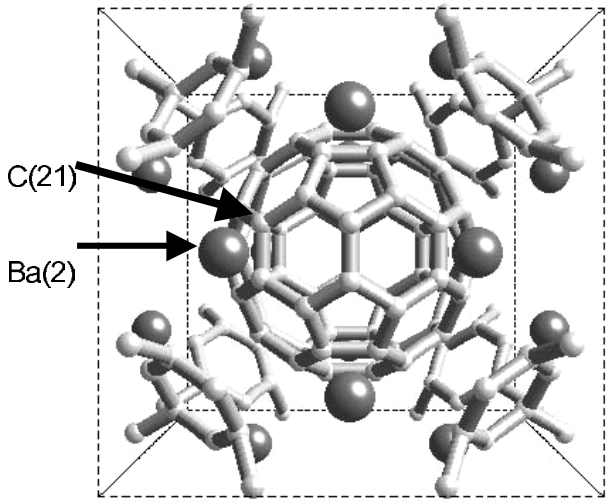

Figure 4. The crystal structure of superconducting Ba_4C_{60} viewed from the [001] direction.

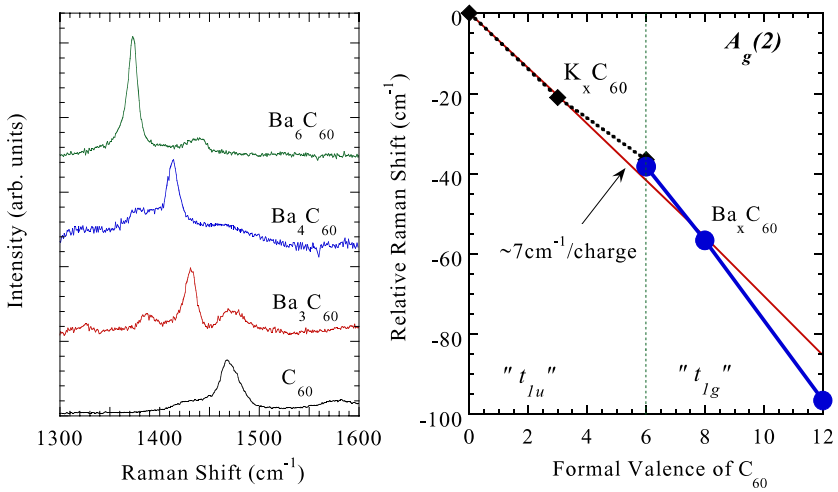

Figure 5. Left: Raman spectra for pristine and Ba-doped C_{60} in the region near the pentagonal pinch mode. The highest peak is assigned as the $A_g(2)$ mode. Right: the Raman shift in wavenumber of the $A_g(2)$ mode versus the formal valence of C_{60}. Diamonds and circles correspond to K-doped and Ba-doped C_{60} compounds respectively. The formal valence of C_{60} is estimated assuming the ionic crystal model, where complete charge transfer from divalent Ba ions and monovalent K ions to C_{60} occurs.

been achieved in binary compounds, partly because the reaction of rare-earth elements such as La and Ce, which could be trivalent, has not been successful due to the low vapour pressure. $A_3Ba_3C_{60}$ is synthesized by reaction of alkali metals with preformed Ba_3C_{60}. The crystal structure is identical to those of Ba_6C_{60} and K_6C_{60}, with the space group $Im\bar{3}$. The structure of $A_3Ba_3C_{60}$ is the solid solution of these two end compounds. Importantly, this nonavalent phase shows superconductivity with a maximum T_c of 5.6 K.

Another possible superconducting ternary system is $K_2Ba_4C_{60}$. The process of synthesis of this compound is similar to that for $K_3Ba_3C_{60}$: excess potassium is intercalated into preformed

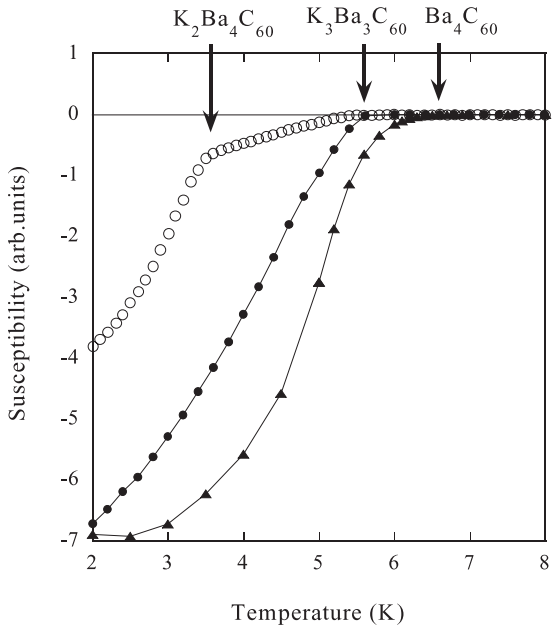

Figure 6. The temperature dependence of the zero-field-cooled magnetic susceptibility for Ba_4C_{60} (filled triangles), $K_3Ba_3C_{60}$ (filled circles), and $K_2Ba_4C_{60}$ (open circles).

Ba_4C_{60}. Figure 6 shows the temperature dependence of the magnetic susceptibility for Ba_4C_{60}, $K_3Ba_3C_{60}$, and $K_2Ba_4C_{60}$. The superconductivity signal of Ba_4C_{60}, with $T_c = 6.7$ K, immediately disappears upon doping with K, displaying two onsets of superconductivity. One is at 5.6 K, which is attributable to $K_3Ba_3C_{60}$. Since Ba_4C_{60} always contains a small amount (a few per cent at most) of stable Ba_3C_{60} as a minority phase, the formation of $K_3Ba_3C_{60}$ is inevitable. We observed another onset of a diamagnetic signal at 3.6 K, which should be attributed to $K_2Ba_4C_{60}$. The volume fraction of this superconducting phase reaches 14%, indicating that this is a bulk superconductor.

To identify the superconducting phase, a high-resolution x-ray diffraction pattern was recorded at a synchrotron radiation facility, KEK-PF, BL1B, and is shown in figure 7. The structure is again identical to the bcc K_6C_{60} and Ba_6C_{60} ones, with the space group $Im\bar{3}$ and the lattice parameter $a = 11.212$ Å. This parameter is in between those of $K_3Ba_3C_{60}$ and Ba_6C_{60}, indicating that the compound has an intermediate composition. A Rietveld structural analysis has revealed that the refined chemical composition is $K_{1.79(1)}Ba_{4.20(1)}C_{60}$. Here, the sum of the K and Ba concentrations was constrained to be 6, to reduce the number of independent parameters. The same analysis on the nominal $K_3Ba_3C_{60}$ phase with $T_c = 5.6$ K, carried out to provide a reference, gave $K_{2.99(1)}Ba_{3.01(1)}C_{60}$, showing reasonable and systematic variations. The results of the Rietveld analysis of nominal $K_3Ba_3C_{60}$ and $K_2Ba_4C_{60}$ are summarized in table 2. On the basis of the magnetic and structural characterization, we conclude that intercalation of Ba_4C_{60} with K produces another superconducting phase: $K_2Ba_4C_{60}$ with $T_c = 3.6$ K. The nominal valence of C_{60} in $K_2Ba_4C_{60}$ is $(C_{60})^{-10}$.

Now, superconductors of several types in the t_{1g} band are established: octavalent Ba_4C_{60} and Sr_4C_{60} (bco), nonavalent $K_3Ba_3C_{60}$ (bcc), and decavalent ($K_2Ba_4C_{60}$ (bcc), Ca_5C_{60} (simple cubic)) fullerides. The occurrence of superconductivity in materials with different band fillings and crystal structures is in sharp contrast with the case for t_{1u} superconductors which are, in

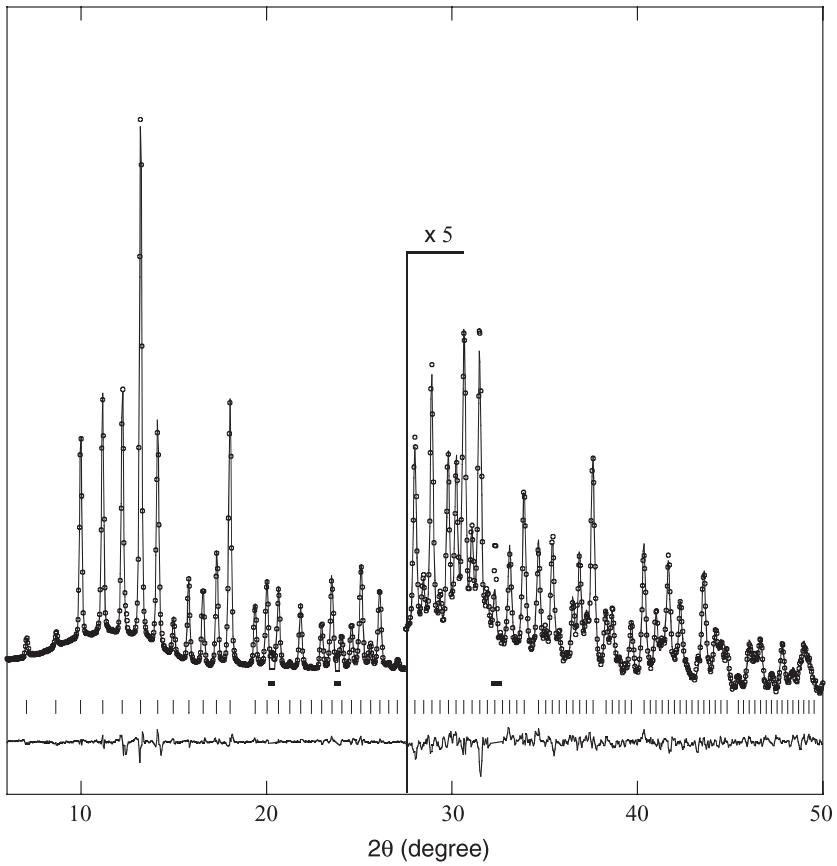

Figure 7. A synchrotron x-ray diffraction pattern for nominal $K_2Ba_4C_{60}$ for the wavelength of 0.688 81(3) Å. Open circles and solid lines show observed and calculated patterns, respectively. The deviations between these two data sets are displayed at the bottom. Ticks mark the positions of the Bragg reflections. The results of the analysis are summarized in table 2.

principle, restricted to the fcc A_3C_{60} group. Among these materials, a systematic investigation has been made on the $A_3Ba_3C_{60}$ system.

T_c for this system is plotted against the bcc lattice parameter in figure 8. T_c decreases as a function of lattice parameter, in sharp contrast to the well-known case for A_3C_{60}, where T_c is an increasing function of the lattice parameter. Measurements of the magnetic susceptibility revealed that the low T_c compared to those of A_3C_{60} compounds is predominantly attributable to the low density of states at ε_F. From magnetic susceptibility experiments, the value of $N(\varepsilon_F)$ was obtained as 5.7 and 4.1 states $eV^{-1}/(C_{60}$ spin) for $K_3Ba_3C_{60}$ and $Rb_3Ba_3C_{60}$, respectively. These values are considerably lower than that for K_3C_{60}(13 states $eV^{-1}/(C_{60}$ spin)). It is noted that the value of $N(\varepsilon_F)$ for $Rb_3Ba_3C_{60}$, with larger interfullerene spacing, is smaller than that for $K_3Ba_3C_{60}$ [26]. The decrease of T_c as a function of the lattice parameter in $A_3Ba_3C_{60}$ is ascribed to the reduction of the density of states, in accord with the BCS picture. However, the naïve band picture, in which the density of states decreases with increasing interfullerene distance, does not hold in the $A_3Ba_3C_{60}$ system, in contrast to the case for A_3C_{60} superconductors.

Possible explanations for this unusual behaviour are given by a first-principles band calculation and a detailed structural study. The former made a comparison of the densities

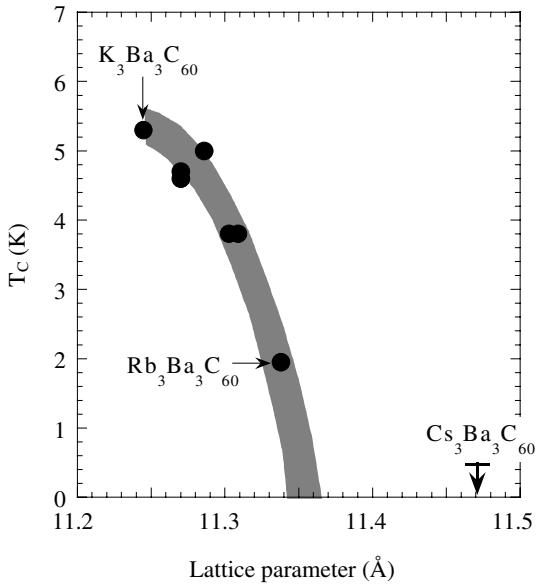

Figure 8. A plot of T_c versus the bcc lattice parameter for the $A_3Ba_3C_{60}$ system with nominal valence $n = 9$.

Table 2. Results of the Rietveld refinement of the x-ray powder diffraction of $K_3Ba_3C_{60}$ and $K_2Ba_4C_{60}$ superconductors.

		$K_3Ba_3C_{60}$			
Lattice parameters (Å)			11.2360(1)		
Space group			$Im\bar{3}$		
R-factors (%)			$R_p = 3.05$, $R_{wp} = 3.14$		
Atomic coordinates and thermal parameters		x	y	z	B (Å^2)
	C(1)	0.064 4(1)	0.000 00	0.3090(1)	0.016(1)
	C(2)	0.128 7(1)	0.104 9(2)	0.2718(1)	0.016(1)
	C(3)	0.063 3(2)	0.205 2(1)	0.2330(2)	0.016(1)
	Ba^{+2}	0.000 00	0.500 00	0.2797(2)	0.023(1)
	K^{+1}	0.000 00	0.500 00	0.2797(2)	0.023(1)
Refined composition			$K_{2.99(1)}Ba_{3.01(1)}C_{60}$		
		$K_2Ba_4C_{60}$			
Lattice parameters (Å)			11.2122(1)		
Space group			$Im\bar{3}$		
R-factors (%)			$R_p = 2.65$, $R_{wp} = 3.05$		
Atomic coordinates and thermal parameters		x	y	z	B (Å^2)
	C(1)	0.063 9(1)	0.000 00	0.3097(2)	0.016(1)
	C(2)	0.132 3(1)	0.103 3(2)	0.2727(1)	0.016(1)
	C(3)	0.061 5(2)	0.206 8(2)	0.2318(1)	0.016(1)
	Ba^{+2}	0.000 00	0.500 00	0.2808(3)	0.023(1)
	K^{+1}	0.000 00	0.500 00	0.2808(3)	0.023(1)
Refined composition			$K_{1.79(1)}Ba_{4.20(1)}C_{60}$		

of states at ε_F for $K_3Ba_3C_{60}$ and $Rb_3Ba_3C_{60}$, and showed that, due to the hybridization of Ba and carbon orbitals, the naïve picture is not appropriate in the case of $A_3Ba_3C_{60}$. In fact, the calculated densities of states for $K_3Ba_3C_{60}$ and $Rb_3Ba_3C_{60}$ are almost identical [46]. The latter experiment revealed that the atomic positions of K and Ba are slightly different, causing a local distortion in the solid-solution structure of $A_3Ba_3C_{60}$ [47]. Although the ionic radii of K^+ and Ba^{2+} are very similar, Rb^+ and Cs^+, which have larger ionic radii, induce more serious distortion in the structure. This may explain the reduction of T_c in this system. More investigations are still necessary for a deeper understanding of this system.

As a brief summary of the properties of t_{1g} superconductors, we can say that doping with alkaline-earth metals often yields C_{60} superconductors that have a full t_{1u} conduction band and a partially filled t_{1g} conduction band. It seems that there are no particular rules for the occurrence of superconductivity. Superconductivity is observed in various crystal structures, such as orthorhombic, bcc, and fcc-derived simple cubic. Also there is no strict regulation of the nominal valence state. Superconductivity seems to be achieved once partial filling of the t_{1g} band is obtained. The value of $N(\varepsilon_F)$ for the t_{1g} system is considerably smaller than that for t_{1u} superconductors, resulting in the low T_c, below 8 K. All these situations suggest that the band picture is successful for all the band-filling states in the t_{1g} system.

3. Electronic properties of the t_{1u} states

Superconductivity in the t_{1u} states has been observed in alkali-metal-doped C_{60} with the composition A_3C_{60} and in rare-earth-metal-doped C_{60}, $Yb_{2.75}C_{60}$, and $Sm_{2.75}C_{60}$. Since the understanding of the latter system is quite poor at this moment, we will focus our attention on the former system in this section. There are several important features of the A_3C_{60}-type superconductors:

(1) $n = 3$ is the sole electron filling state which yields superconductivity in the alkali-metal-doped systems.
(2) Superconductivity in the $n = 3$ state appears exclusively in the fcc and fcc-derived simple cubic structures.
(3) The band model + BCS picture seems quite successful for the $n = 3$ superconductors.

The success of both the band model and the BCS picture is of particular importance, since they provided a simple guideline for improving T_c: if the interfullerene spacing is expanded, the transfer energy or bandwidth becomes smaller. Consequently, the density of states at the Fermi energy $N(\varepsilon_F)$ is enhanced, causing the improvement of T_c (figure 3). These situations are well described in the former review articles [31–33].

However, we would like to stress that this band model + BCS picture is valid only for the $n = 3$ state and fcc structures. It is of particular importance to the BCS-based superconductivity that the normal state is metallic in a manner consistent with the band model, which predicts metallic states for partially filled conduction bands. Nonetheless, the breakdown of the band model is frequently observed in the t_{1u} states, in contrast to the case for the t_{1g} system. In this section, we describe one example of failures in the band model of C_{60} solids.

K_4C_{60}, a neighbouring compound of superconducting K_3C_{60}, is known to be an insulating material, in contradiction to the band picture prediction [48–50]. Since the filling of the LUMO is partial ($n = 4$) in K_4C_{60}, a metallic state is anticipated in the same way as for K_3C_{60}. A band structure calculation, taking the tetragonal structure of K_4C_{60} into account, also predicts a metallic state [51]. Nonetheless, the semiconducting nature of K_4C_{60} has been consistently observed in experiments of various kinds from the very early stages of solid-state fullerene research [48–50], and the mechanism of the failure of the band calculation for this material, as

Figure 9. Possible Jahn–Teller splitting of the triply degenerate LUMO states for Na_2C_{60} ($n = 2$) and K_4C_{60} ($n = 4$).

well as the absence of superconductivity, is not fully understood. More recently, another important insulating state has been discovered in Na_2C_{60}. This compound adopts an fcc structure in which two tetrahedral sites are occupied by Na ions, while the octahedral hole is unoccupied [52]. This system is also expected to be metallic and superconducting because of the partial filling of the LUMO band, and also because the structure is almost identical to that of the superconducting phase K_3C_{60}. Nonetheless, Na_2C_{60} turns out to be nonsuperconducting, and recent magnetic experiments revealed that it is not even metallic, but semiconducting [53, 54].

A common feature of Na_2C_{60} and K_4C_{60} is that the semiconducting states of both compounds are magnetically inactive (*nonmagnetic* or spin singlet). The nonmagnetic semiconducting states for these two compounds are most probably explained by the Jahn–Teller effect, where spontaneous deformations of high-symmetry molecules induce the splitting of degenerate levels to gain the electronic energy. On removing degeneracy, both even-numbered valence states ($n = 2$ and 4) become singlet states, resulting in semiconducting solids (figure 9). The Jahn–Teller-type electron–phonon interaction S is strong enough in C_{60} solids to destroy the band picture for particular valence states. In fact, Jahn–Teller distortions of C_{60} molecules have been directly found by structural analysis of single crystals, such as $(NH_3)_8BaC_{60}$ [55] and $[PNN]_3C_{60}$ (PNN = *bis*(triphenylphosphine)iminium) [56] single crystals with divalent and trivalent C_{60}, respectively, both in isolated states. Although electron energy loss spectra of Na_2C_{60} and even-valence C_{60} compounds revealed that the nature of the electronic gap is dominated by the on-ball Coulomb repulsion U, the nonmagnetic ground states can be understood only when S is taken into account [57].

Experimental evidence of the Jahn–Teller distortion was first provided from the infrared conductivity spectra for K_4C_{60}, exhibiting splitting of the T_{1u} intramolecular phonon [44]. This splitting could be understood in terms of reduction of molecular symmetry. However, structural confirmations remain to be carried out for the Na_2C_{60} and K_4C_{60} systems, predominantly due to the orientationally disordered structures. Very recently, structural analysis of powder neutron diffraction data uncovered Jahn–Teller distortion of C_{60} molecules in Cs_4C_{60}—taking advantage of the fully orientationally ordered structure [58].

4. Comparison of t_{1u} and t_{1g} states

When comparing properties of t_{1u}- and t_{1g}-based materials, one may find the following notable differences:

(1) The value of $N(\varepsilon_F)$ for the t_{1g} band is considerably smaller than those for the t_{1u} band.
(2) Once the t_{1g} band is partially filled, the metallic state and superconductivity are simultaneously achieved (Ba_4C_{60}, $K_3Ba_3C_{60}$, $K_2Ba_4C_{60}$ and Ca_5C_{60}). However, T_c, for this group of compounds, is 8 K at maximum.
(3) In the t_{1u} states, the metallic/superconducting states are often destroyed and both nonmagnetic and magnetic (as shown in the following sections) insulating states are observed.

(4) Superconductivity is found exclusively in the trivalent state for the t_{1u} states, and T_c reaches more than 30 K.

An important difference between the electronic properties of the t_{1u} and t_{1g} states is as regards the stability of the metallic states. It seems that the metallic state is quite stable in the t_{1g} band, whereas it is often destroyed in the t_{1u} band. In other words, there are several instabilities against insulating states in the alkali-metal-doped systems, while such instability is absent in Ba-rich systems. This is one of the most fundamental issues relating to the doped fullerides. In particular, isostructural compounds, such as Ba_4C_{60} and its alkali metal analogue A_4C_{60}, provide an important opportunity for comparative study, because they are basically isostructural with partially filled t_{1g} and t_{1u} bands, respectively. Ba_4C_{60} is a superconductor with $T_c = 6.7$ K, while K_4C_{60}, Rb_4C_{60}, and Cs_4C_{60} are all nonmagnetic insulators. (Strictly speaking, only Cs_4C_{60} is isostructural with Ba_4C_{60} [44], and K_4C_{60} and Rb_4C_{60} are tetragonal due to the merohedral disordering of the C_{60} molecules. But this difference does not play an essential role in the electronic states.)

A clue is obtained by a careful examination of the crystal structure shown in figure 4. It was found that there are some very small interatomic distances between barium and carbon [24]—in particular, the distance between Ba(2) and C(21) is 2.990(4) Å, which is almost identical to the sum of the ionic radius of Ba^{2+} and the van der Waals distance of carbon. This small distance is strongly suggestive of very strong hybridization of Ba(5d) and C(2p) orbitals, which could broaden the bandwidths. The increase of the bandwidth [59] suppresses several instabilities against the insulating states. This speculation is also supported by first-principles band calculations for Ba_6C_{60}, where the hybridization of Ba and C orbitals plays an important role in the band broadening [60, 61]. Also, the experimentally obtained density of states at the Fermi energy in Ba_4C_{60} is significantly smaller than those of alkali-metal-doped C_{60} superconductors [24].

Such orbital hybridization implies that the ionic crystal model, which assumes the complete charge transfer from metals to C_{60}, is not valid any longer in Ba-doped systems. However, considering the almost continuous Raman shift shown in the right-hand panel of figure 5, the model of complete charge transfer works reasonably well, and the hybridization effect is not so dominant. Importantly, such a small hybridization is sufficient for stabilizing the metallic states.

5. The Mott–Hubbard transition in the $(NH_3)A_3C_{60}$ system

A different type of breakdown of the band picture for the t_{1u} band is seen in a chemical derivative of a trivalent superconductor, K_3C_{60}. Among the nonsuperconducting compounds, $(NH_3)K_3C_{60}$ is the most intriguing and informative system, displaying typical characteristics of breakdown of the band picture. Figure 10 shows a schematic representation of the crystal structure of K_3C_{60} and $(NH_3)K_3C_{60}$. A neutral ammonia molecule is inserted in an octahedral site of K_3C_{60}, causing a slight distortion of the lattice into an orthorhombic form [15].

A variety of experiments have been performed on $(NH_3)K_3C_{60}$ and it was found that the ground state of $(NH_3)K_3C_{60}$ is again an insulator, but, in this case, *magnetic*. The first evidence was provided by ESR measurements. The left-hand panel of figure 11 displays ESR spectra at room temperature for an isostructural series of $(NH_3)K_{3-x}Rb_xC_{60}$ compounds obtained by alloying the alkali metal site [62]. The ESR spectra were found to become broader with increasing Rb concentration. Similar broadening, encountered in ESR spectra for A_3C_{60} compounds, has been understood in terms of enhanced spin–orbit interaction in Rb ions. The spin susceptibility can be estimated by double integration of the ESR spectra

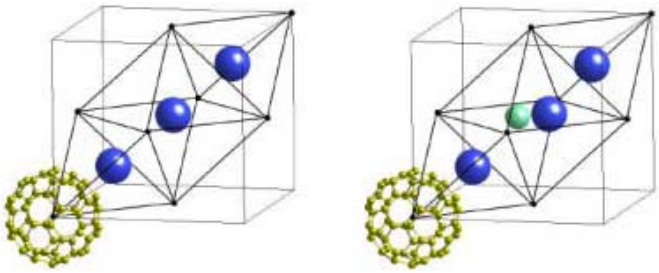

Figure 10. Schematic crystal structures of K_3C_{60} and $(NH_3)K_3C_{60}$. Large and small spheres represent K ions and NH_3 molecules, respectively. C_{60} molecules, residing at the face-centred positions, are displayed as small dots. Each tetrahedral and octahedral site is occupied by a single K ion.

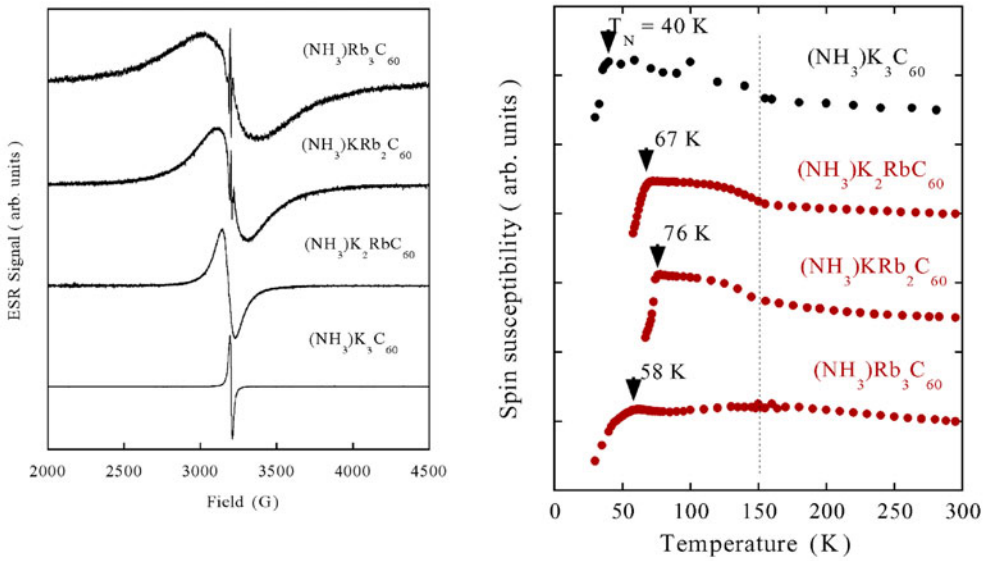

Figure 11. Left: room temperature ESR spectra for $(NH_3)A_3C_{60}$ compounds at 9 GHz. The increase of the ESR linewidth with the Rb fraction is ascribed to the enhanced spin–orbit interaction in Rb ions. Right: the temperature dependence of the ESR intensity for $(NH_3)A_3C_{60}$ compounds. The rapid decrease in intensity marked by arrows indicates the occurrence of antiferromagnetic ordering. The weak anomaly at 150 K (shown by the dotted line) is a sign of a structural phase transition associated with the orientational order of C_{60} and A–NH_3 groups.

in figure 11. The temperature dependence of the ESR intensity (which is proportional to the spin susceptibility in the paramagnetic state) is displayed in the right-hand panel of figure 11. Importantly, the ESR intensity for all four compounds rapidly decreases with temperature, as marked by arrows. This intensity drop is associated with the broadening of the ESR linewidth, indicating that the transition is an antiferromagnetic ordering, by analogy with that in A_1C_{60} [37]. The subsequently performed μSR [40], high-field ESR [41], and NMR experiments [42] on $(NH_3)K_3C_{60}$ confirmed that the drop in the ESR signal is ascribable to antiferromagnetic long-range ordering.

In particular, the oscillatory relaxation curve obtained in the μSR experiment provided the first confirmation of antiferromagnetic long-range order in $(NH_3)K_3C_{60}$. Prassides *et al* [40] also suggested that the magnetic moment on the C_{60} moiety is close to $S = 1/2$. ^{13}C

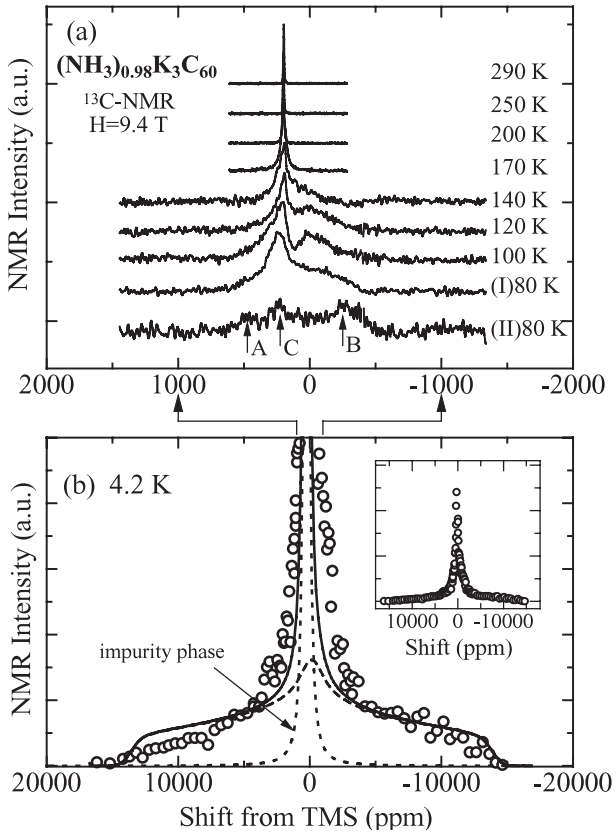

Figure 12. ^{13}C NMR spectra of $(NH_3)K_3C_{60}$ at various temperatures. The top panel (a) shows the spectra for paramagnetic states. The bottom panel (b) shows a spectrum for an antiferromagnetic state. In (b), the experimental data are shown as open circles and the solid line represents a best fit to a model calculation. The fit is a sum of the intrinsic (dashed curve) and impurity (dotted curve) signals.

NMR spectra and their temperature variation are shown in figure 12 [42]. NMR data include information not only on magnetic but also on rotational states of the C_{60}. At 300 K, a single-peaked spectrum is observed, indicative of the rotation of C_{60} molecules. The spectral broadening below $T_S = 150$ K is evidence for freezing of rotation, which will be discussed in the next section. The tremendous spectral broadening at 4.2 K (shown in the bottom panel of figure 12) provided direct evidence for the antiferromagnetic ordering. The low-spin ($S = 1/2$) state of C_{60} molecules was found from careful analyses of the NMR spectra and the temperature dependence of the relaxation rate T_1^{-1}.

Figure 13 summarizes the Néel temperature T_N (determined by ESR data) for the $(NH_3)A_3C_{60}$ system together with T_c for A_3C_{60} superconductors. This phase diagram clearly shows that the superconductivity in A_3C_{60} is replaced by antiferromagnetic state in the ammoniated systems, and that these two states are close to each other in terms of volume (or interfullerene distance). Proximity of superconductivity and magnetic states has been seen in various materials, including oxide superconductors, organic compounds, and heavy-fermion systems, where the electron correlation effect plays crucial roles not only in the magnetic state but also in the superconducting state. Since the superconductor–antiferromagnet transition is associated with the structural distortion in the case of ammoniated fullerides, the situation is not

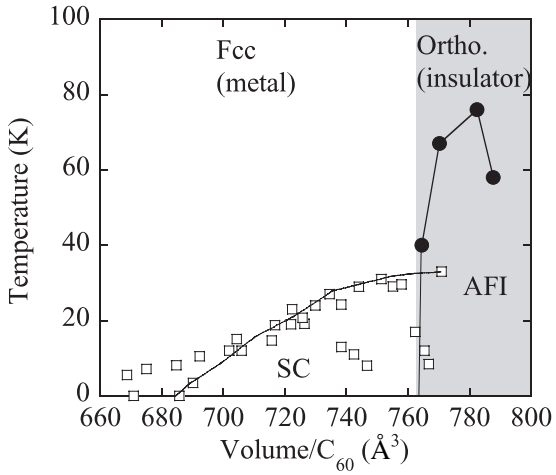

Figure 13. The electronic phase diagram of trivalent fullerides. The hatched region shows the orthorhombic insulator phase. SC and AFI denote the superconducting state and antiferromagnetic insulating state, respectively. Open squares and filled circles show the critical temperatures for superconductivity (T_c) and antiferromagnetic order (T_N), respectively.

straightforward as in the case of other strongly correlated materials. However, the appearance of antiferromagnetic states in the vicinity of the superconductors shown in figure 13 indicates that the electron correlation is very large also in the trivalent states. Furthermore, T_N reaches 76 K in $(NH_3)KRb_2C_{60}$, which is the highest value among molecule-based materials without magnetic elements. Such a high magnetic ordering temperature is another notable aspect of fullerene-based solids.

According to the band calculation, $(NH_3)K_3C_{60}$ is expected to be metallic regardless of the structural deformation, because of its odd valence n (=3) [63]. Also, since the volume per C_{60} is comparable to that for the Rb_2CsC_{60} superconductor with $T_c = 31$ K, this compound was first anticipated to be superconducting with $T_c > 30$ K. Hence, the insulating and magnetic state of $(NH_3)K_3C_{60}$ is quite surprising and, thus, of particular importance. Such magnetic insulators are known as Mott insulators, where the electrons are localized because of the large on-ball Coulomb interaction U between electrons. The key issue is when the electron localization takes place. At first, the metal–insulator transition was believed to take place at low temperatures, presumably at the Néel temperature or at the structural transition temperature, 150 K (which will be described later). This is partly because the spin susceptibility is approximately temperature independent, as shown in figure 11. Since the ammoniated alkali fulleride samples are obtained only in an air-sensitive powder form, direct measurements of conductivity and optical measurements were not carried out on this compound until very recently, although these are very important physical quantities. Kitano and co-workers [64] determined the ac conductivity at 9 GHz for this series of compounds using a cavity perturbation technique. Figure 14 displays the conductivity for several ammoniated fullerides at 250 K. K_3C_{60} and $(NH_3)_xNaRb_2C_{60}$ compounds, which afford fcc structures and become superconducting, show high conductivity values of the order of 10^2–10^3 S cm^{-1}. In sharp contrast, the conductivity of the orthorhombic $(NH_3)K_{3-x}Rb_xC_{60}$ series is 3–4 orders of magnitude smaller than that of the superconducting fcc fullerides. Since the conductivity measurement is made at 250 K, well above T_N and the structural transition temperature, the low conductivity should be attributed not to these phase transitions, but to the slight distortion in crystal structure from fcc to face-

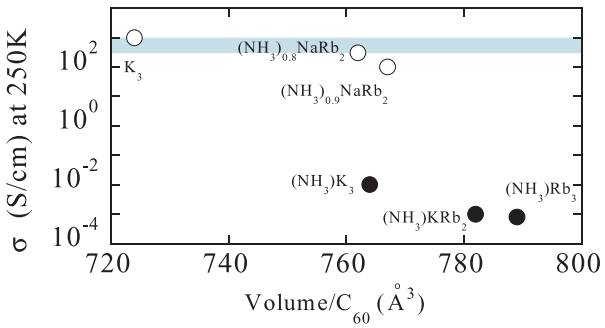

Figure 14. Microwave conductivity at 250 K against volume/C_{60}. Open and full circles represent cubic and orthorhombic fullerides, respectively. The hatched line shows the Mott limit. The conductivity decreases very slightly with increasing volume/C_{60} or interfullerene spacing within isostructural compounds. The dramatic reduction of conductivity (the metal–insulator transition) is associated with the structural change from cubic to orthorhombic.

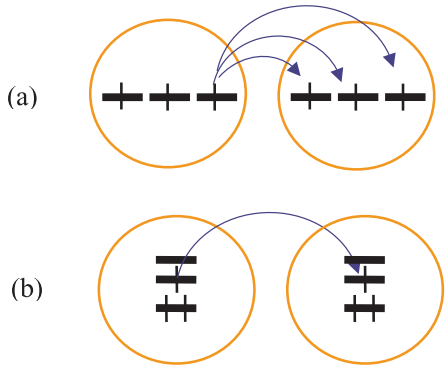

Figure 15. Models of the charge transfer between trivalent molecules with triply degenerate molecular orbitals (a) and without degeneracy (b) at $T = 0$ K. In the former case, there are three hopping channels, in contrast to the one hopping channel in the latter case.

centred orthorhombic. In other words, this Mott–Hubbard transition is induced by symmetry reduction of the crystal structure.

Here, we should take into account the triple degeneracy of the t_{1u} molecular orbital, where three electrons are doped. In principle, this degeneracy and high-symmetry fcc structure is crucial to realizing metallic states in fullerides, as was pointed out by Lu [65] and Gunnarsson *et al* [66]. Figure 15 shows an illustration intended to explain the effect of triple degeneracy. In the cubic crystal field, the triple degeneracy is maintained; there are three channels for electron hopping (figure 15(a)). In contrast, when there is a structural distortion, the degeneracy is lifted, so we have only one hopping channel for electrons if one considers the electron transport at $T = 0$ K (figure 15(b)). This simple consideration indicates that the structural distortion causes band narrowing, which may result in a metal–insulator transition when the bandwidth W is comparable to U. Also, the splitting of the level in figure 15(b) is consistent with the low-spin state ($S = 1/2$) observed in the μSR and NMR studies of $(NH_3)K_3C_{60}$.

Within a band picture, a large distortion is required to induce splitting of the conduction band. However, a recent theory given by Manini and co-workers [63] showed that even a tiny distortion is sufficient for causing the electron localization when the system is on the verge of

the Mott–Hubbard transition. In fact, the U-value is believed to be rather large even in A_3C_{60} superconductors. Several estimations have shown that $U \sim 1$ eV, the bandwidth $W \sim 0.5$ eV, and the Jahn–Teller-type electron–phonon interaction $S \sim 0.2$ eV. These estimates imply that these important energy scales are competing in intercalated fullerides, and that this is the most essential point for various electronic states such as the superconducting, Jahn–Teller insulating, and Mott–Hubbard insulating ones occurring in fullerides [33, 67]. Hence the superconductivity of A_3C_{60} fullerides is very fragile against valence shift or structural distortion.

6. Molecular orbital order in the $(NH_3)A_3C_{60}$ system

We have shown in the previous section that the orthorhombic $(NH_3)A_3C_{60}$ system is a Mott–Hubbard insulator with electrons localized on C_{60} molecules that undergo antiferromagnetic ordering. Another unique aspect to be stressed is the rotational degree of freedom of the C_{60} molecule. In this section, we will describe how C_{60} rotation plays a very important and interesting role in controlling the intermolecular magnetic interaction in the $(NH_3)A_3C_{60}$ system.

Figure 16 summarizes phase transformation sequences for C_{60}, K_3C_{60}, and $(NH_3)K_3C_{60}$. The plasticity of undoped C_{60} is well known: above the fcc–simple cubic structural transition at 260 K, C_{60} molecules rotate freely. Below 260 K, molecules show a jumping motion between several stable orientations [68, 69]. This is called ratcheting. When temperature is further reduced, a glass transition takes place at 90 K, below which all rotations are frozen in a disordered fashion. In doped fullerides, on the other hand, rotation of C_{60} molecules is substantially hindered. In particular, when larger cations are introduced, as in K_6C_{60}, no molecular rotation is observed. For concentrations of smaller cations, such as K_3C_{60}, there is no free rotation, but ratcheting is allowed at room temperature. Freezing of the ratcheting motion takes place as a continuous crossover around 200 K [70]. Thus the low-temperature state of K_3C_{60} is orientationally disordered. Despite this disorder, superconductivity does arise in K_3C_{60} and related compounds, indicating that superconductivity of fullerides is robust against rotational disorder. The structural transition sequence of $(NH_3)A_3C_{60}$ is very similar to that of K_3C_{60}, but in contrast to K_3C_{60} showing orientational disorder, the low-temperature state of $(NH_3)A_3C_{60}$ is orientationally *ordered*.

Figure 17 shows the expanded diffraction pattern of $(NH_3)K_3C_{60}$ at 15 and 300 K [71]. Arrowed peaks in the 15 K pattern are forbidden reflections in the $Fmmm$ space group at 300 K. All these peaks were successfully indexed as half-integers, indicating that the unit cell is doubled at low temperature with the space group $Fddd$. Figure 18 displays the temperature dependence of the normalized intensity of superlattice peaks. The critical behaviour of the superlattice intensity below $T_S = 150$ K unambiguously shows the occurrence of the second-order phase transition. It is also noted that the same phase transition is observed at the same temperature of $T_S = 150$ K in all other $(NH_3)A_3C_{60}$ compounds. This structural transition has been detected by ESR measurements, as shown in figure 11.

The crystal structure in the low-temperature phase was determined by a Rietveld analysis of the full powder x-ray diffraction pattern [71]. The occurrence of cell doubling was well accounted for by the orientational ordering of K–NH_3 groups, indicating that not only the C_{60} but also the K–NH_3 behave as rotors at temperatures higher than T_S. The low-temperature structure of $(NH_3)K_3C_{60}$ is displayed in the left-hand panel of figure 19. NH_3–K groups are aligned in a ferroelectric fashion along the (110) direction. Although the orientational state of C_{60} was not determined by the x-ray diffraction study, Margadonna *et al* [72] have succeeded in determining the orientational order of C_{60} molecules by means of neutron diffraction and

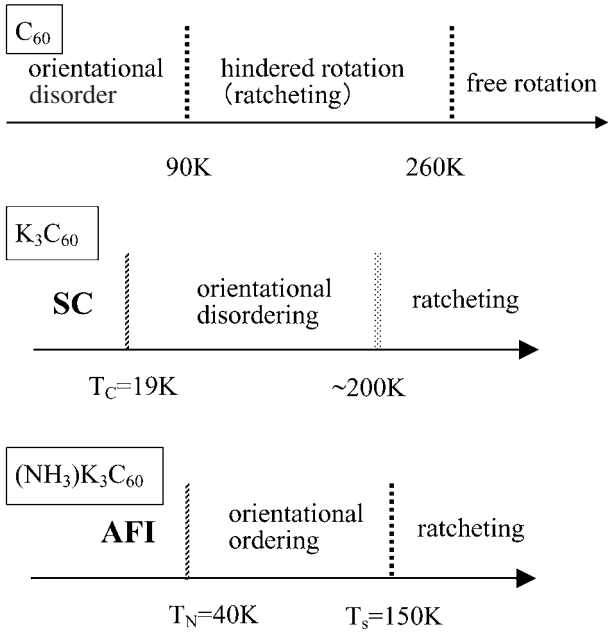

Figure 16. The sequence of structural and electronic phase transitions in C_{60}, K_3C_{60}, and $(NH_3)K_3C_{60}$.

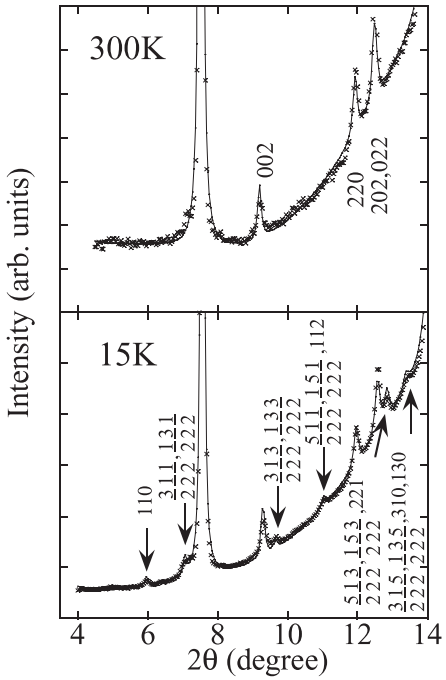

Figure 17. Low-angle x-ray powder diffraction profiles of $(NH_3)K_3C_{60}$ at 300 and 15 K. Superlattice peaks indexed as half-integers appear at low temperature.

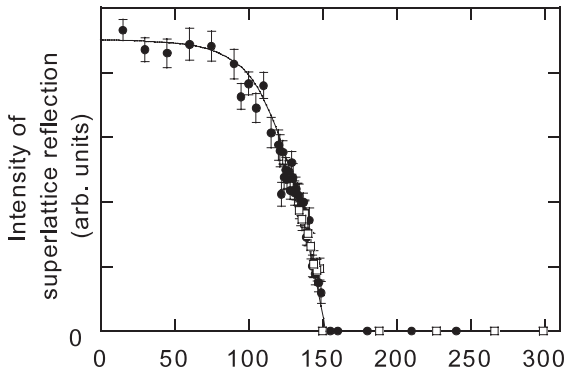

Figure 18. The temperature dependence of the normalized intensity of the superlattice reflections indexed as half-integers in figure 17.

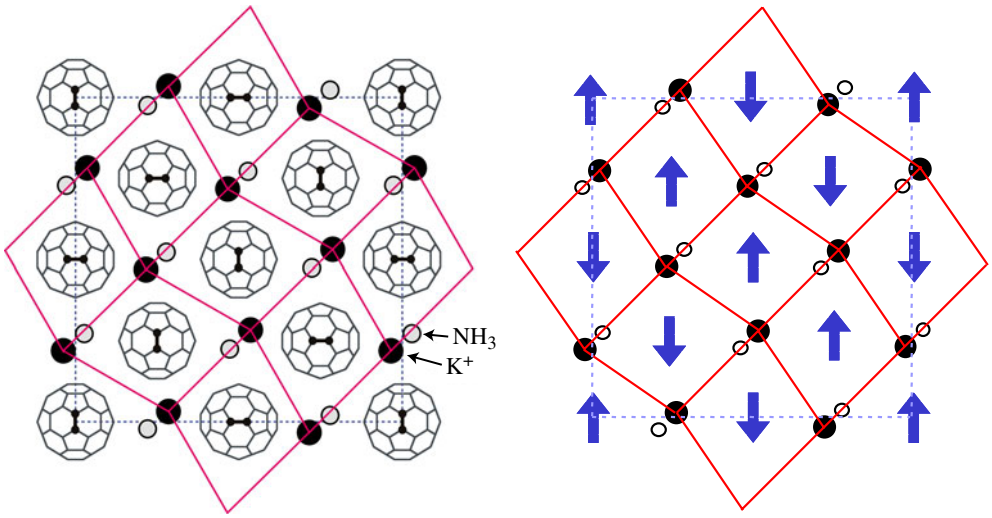

Figure 19. Schematic representations of the crystal structure (left) and magnetic structure (right) for $(NH_3)K_3C_{60}$. Solid lines indicate octahedra of K ions surrounding C_{60} molecules.

Rietveld analysis. They found that, associated with the ordering of K–NH_3 groups, the rotation of C_{60} is also ordered: ferro-rotationally along the [110] direction and antiferro-rotationally along the $[1\bar{1}0]$ direction. The ordering of K–NH_3 groups causes the distortion of the octahedra of K ions that surround C_{60} molecules, as shown in the left-hand panel of figure 19. We presume that this distortion induces the noncubic local potentials on C_{60}, and, consequently, that the C_{60} molecule is orientationally ordered. In the case of K_3C_{60}, on the other hand, the local potential from the undistorted octahedra remains cubic, resulting in orientational disorder of C_{60}. The second-order structural transition in $(NH_3)A_3C_{60}$, in contrast to the crossover in K_3C_{60}, is ascribed to the cooperative freezing of two rotors (C_{60} and the NH_3–A group).

The dynamical aspect of the structural phase transition was detected from the ^{13}C NMR spectra (figure 12). The single-peaked spectrum at 300 K, followed by spectral broadening below $T_S = 150$ K, indicates that the molecular rotation at room temperature is stopped, in a similar manner to the case for undoped C_{60} and K_3C_{60}. More importantly, NMR data provide crucial information on magnetic properties. For instance, the huge broadening of ^{13}C spectra

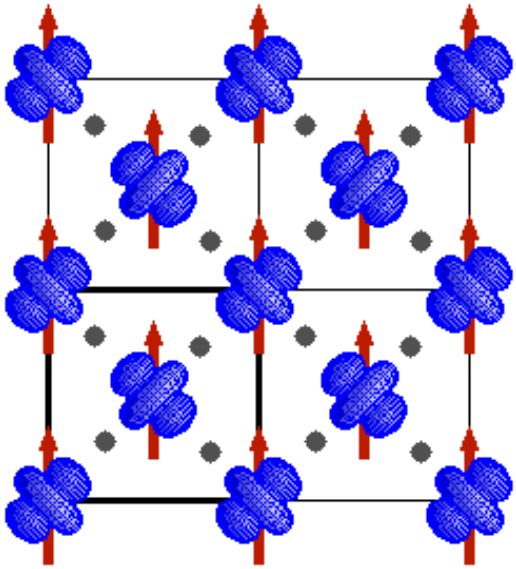

Figure 20. Orbital and magnetic order in $LaMnO_3$, which provides an analogy with the correlation between molecular orientation and magnetic structures in $(NH_3)K_3C_{60}$. Clouds and arrows show d orbitals and spins of Mn^{3+}, respectively.

in figure 12 is one of the most important pieces of evidence for the antiferromagnetic state, as described in the previous section.

Combining spectral analyses of ^{13}C, ^{1}H, and ^{15}N NMR spectra for the antiferromagnetic state, we were able to uniquely determine the magnetic structure from four possible antiferromagnets within a mean-field theory. The spin structure thus obtained is displayed in the right-hand panel of figure 19. In the [110] direction, spins are antiferromagnetically ordered, while in the $[1\bar{1}0]$ direction, spins are aligned ferromagnetically. Here we should note that only relative spin orientations are determined and that the absolute direction of the spin cannot be identified, since the measurement was carried out with powder samples.

When the molecular orientational ordering, determined by structural analyses, is taken into account, we find an intriguing correlation between the molecular orientation of C_{60} and spin structures. When molecules are ferro-rotationally aligned along the [110] direction, the magnetic interaction is antiferromagnetic. On the other hand, when molecules are ordered antiferro-rotationally along $[1\bar{1}0]$, the magnetic interaction is ferromagnetic. In other words, figure 19 indicates that molecular orientations control the magnetic interactions. Such structural and magnetic correlations remind us of the analogy with the Kanamori–Goodenough empirical rule for transition metal oxides, where alternating orbitals produce ferromagnetic interactions, while parallel orbitals produce antiferromagnetic interactions [73]. Figure 20 displays a typical example of a transition metal oxide antiferromagnet, $LaMnO_3$, where the orbital is ordered at $T_S = 780$ K, with antiferromagnetic order following at $T_N = 140$ K. Here we show a (001) basal plane, in which only alternating orbital order, and thus only ferromagnetic interaction, is observed. The correlation between orbital and magnetic order in $LaMnO_3$ provides a nice analogy with the case of $(NH_3)K_3C_{60}$.

In the case of C_{60}, the molecular orientational order is closely related to the ordering of molecular orbitals, since half-filled t_{1u} states have an orbital degree of freedom in structures with high symmetry. In fact, the orthorhombicity in $(NH_3)K_3C_{60}$ is so small that this crystal

is regarded as a quasi-tetragonal structure. Since the molecular orbital is attached to the molecular skeleton, the orientational order of the molecules is regarded as the ordering of molecular orbitals. Tou *et al* [42] pointed out the orbital degree of freedom in $(NH_3)K_3C_{60}$ and named this ordering 'molecular orbital order'. The important point is that such molecular orbital order controls spin structures.

The effect of molecular orientational/orbital order is not specific to the $(NH_3)A_3C_{60}$ system, but perhaps provides a new opportunity to investigate intermolecular magnetic interactions in other C_{60}-based magnets. For instance, several authors have proposed a similar mechanism of magnetic interactions in a C_{60}-based ferromagnet $(TDAE)C_{60}$ with the Curie temperature at 16 K [74] (where TDAE denotes tetrakisdiaminoethylene). This Curie temperature of 16 K is more than one order of magnitude higher than those for other molecule-based ferromagnets without magnetic elements [75]. A new mechanism has been required to explain this anomalously high T_c. According to Kawamoto and co-workers [76], an alternating ordering of Jahn–Teller-distorted molecules should produce ferromagnetic ordering of localized spins on C_{60}. A recent study of the effect of high pressure on T_c seems to support this model [77]. More importantly, the single-crystal structural analysis at low temperature suggests that there exist alternating molecular rotations in one of the columns of C_{60} [78]. However, the relation between molecular orientation and magnetic interactions in $(TDAE)C_{60}$ requires more investigation.

7. Summary

The current status of superconductivity, Mott–Hubbard transitions, and the role of degenerate molecular orbitals in these phenomena has been reviewed. Although most of the research in this field has focused on the physical properties of the superconductivity in A_3C_{60} phases, study of low-T_c superconductors as well as of nonsuperconducting compounds is quite useful for obtaining a comprehensive understanding of fullerene intercalation compounds.

Intercalation of C_{60} with Ba affords several types of superconductor with different valence and crystal structures. Such tolerance in Ba fulleride superconductors is in sharp contrast with the exclusive criteria for superconductivity in alkali-metal-doped C_{60}. T_c for Ba-doped systems is much lower than the highest T_c for A_3C_{60} superconductors. While superconductivity and the metallic states are quite robust in the t_{1g} system, they are quite fragile in the t_{1u} system against symmetry reduction or Fermi energy shift. Such instability in the t_{1u} system is most probably attributable to the intrinsic character of the C_{60} molecule, where both the electron–phonon interaction S and the electron–electron interaction U are of the same order as the bandwidth. However, in the Ba-doped systems, such instability against several insulating states is weakened, and metallic but lower-T_c superconducting states are stabilized due to the effect of hybridization between Ba ions and carbon atoms.

We have shown that, in the physics of t_{1u} states, orbital degeneracy plays various crucial roles, particularly in the metal–insulator transition and insulating states. Regarding the effect of orbital degeneracy, it is noted that reported bulk superconductivity is so far limited to just C_{60}-based compounds, strongly indicating that orbital degeneracy is also related to the dominant mechanism of superconductivity. For instance, Suzuki *et al* [79] have shown that the dynamical Jahn–Teller effect is equivalent to the interorbital tunnelling of Cooper pairs, which is reminiscent of the Suhl–Kondo mechanism of superconductivity in fullerides. We wish to stress that the molecular orbital degeneracy of C_{60} is quite unique, possibly providing a novel kind of 'orbital physics' in molecular systems which have been extensively investigated as d- or f-electron-based systems. Further investigations not only of insulating but also of metallic states of fullerides are required to establish the physics of the p orbitals in intercalated fullerides.

Acknowledgments

The authors thank H Shimoda (University of North Carolina at Chapel Hill), Dam Hieu Chi, T Ito, H Hayashi, T Furudate, S Taga, T Muro, M Kawaguchi (JAIST), K Prassides, C M Brown, S Margadonna (University of Sussex), X H Chen (University of Science and Technology of China), Y Maniwa, H Tou (Tokyo Metropolitan University), K Ishii, H Suematsu (SPring-8), and K Tanigaki (Osaka City University) for collaborative research on the properties of C_{60} intercalation compounds. Synchrotron x-ray diffraction data were recorded at KEK-PF, Tsukuba, SPring-8, Hyogo, and ESRF, Grenoble. Neutron diffraction experiments were carried out at ILL, Grenoble. In particular, experimental support from Y Murakami and H Nakao (Tohoku University), K Kato and M Takata (JASRI), and E Nishibori and M Sakata (Nagoya University) is greatly appreciated. We also wish to express our thanks to T Mitani (JAIST) for his support and encouragement. This work was supported by the Ministry of Education, Culture, Sports, Science, and Technology (MEXT), the Japan Society for Promotion of Science (JSPS), and Japan Science and Technology Corporation (JST), Japan.

References

[1] Krätchmer W, Lamb L C, Fostiropoulos K and Huffman D R 1990 *Nature* **347** 354
[2] Haddon R C, Hebard A F, Rosseinsky M J, Murphy D W, Duclos S J, Lyons K B, Miller B, Rosamilla J M, Fleming R M, Kortan A R, Glarum S H, Makhija A V, Muller A J, Eick R H, Zahurak S M, Tycko R, Dabbagh G and Thiel F A 1991 *Nature* **350** 320
[3] Hebard A F, Rosseinsky M J, Haddon R C, Murphy D W, Glarum S H, Palstra T T M, Ramirez A P and Kortan A R 1991 *Nature* **350** 600
[4] Tanigaki K, Ebbesen T W, Saito S, Mizuki J, Tsai J S, Kubo Y and Kuroshima S 1991 *Nature* **352** 222
[5] Palstra T T M, Zhou O, Iwasa Y, Sulewski P E, Fleming R M and Zegarski B R 1995 *Solid State Commun.* **93** 327
[6] Nagamatsu J, Nakagawa N, Muranaka T, Zenitani Y and Akimitsu J 2001 *Nature* **410** 63
[7] Haddon R C, Perel A S, Morris R C, Palstra T T M and Hebard A F 1995 *Appl. Phys. Lett.* **80** 121
[8] Kosaka M, Tanigaki K, Prassides K, Margadonna S, Lappas A and Brown C M 1999 *Phys. Rev.* B **59** R6628
[9] Tanigaki K, Hirosawa I, Ebbesen T W, Mizuki J, Shimakawa Y, Kubo Y, Tsai J S and Kuroshima S 1992 *Nature* **356** 419
[10] Tanigaki K and Prassides K 1995 *J. Mater. Chem.* **5** 1515
[11] Fleming R M, Ramirez A P, Rosseinsky M J, Murphy D W, Haddon R C, Zahurak S M and Makhija A V 1991 *Nature* **352** 787
[12] Rosseinsky M J, Ramirez A P, Glarum S H, Murphy D W, Palstra T T M, Haddon R C, Hebard A F, Kortan A R, Zahurak S M and Makhija A V 1991 *Phys. Rev. Lett.* **66** 2830
[13] Zhou O, Fleming R M, Murphy D W, Rosseinsky M J, Ramirez A P, van Dover R B and Haddon R C 1993 *Nature* **362** 433
[14] Shimoda H, Iwasa Y, Miyamoto Y, Maniwa Y and Mitani T 1996 *Phys. Rev.* B **54** R15653
A detailed structure determination is given in
Margadonna S, Aslanis E and Prassides K 2002 *J. Am. Chem. Soc.* **124** 10146
[15] Rosseinsky M J, Murphy D W, Fleming R M and Zhou O 1993 *Nature* **364** 425
[16] Zhou O, Palstra T T M, Iwasa Y, Fleming R M, Hebard A F and Sluewski P E 1995 *Phys. Rev.* B **52** 483
[17] Shimoda H, Iwasa Y and Mitani T 1997 *Synth. Met.* **85** 1593
[18] Imaeda K, Khairullin I I, Yakushi K, Nagata M, Mizutani N, Kitagawa K and Inokuchi H 1993 *Solid State Commun.* **87** 375
[19] Imaeda K, Krober J, Inokuchi H, Yonehara Y and Ichimura K 1996 *Solid State Commun.* **99** 479
[20] Kortan A R, Kopylov N, Glarum S, Gyorgy E M, Ramirez A P, Fleming R M, Thiel F A, Trevor P L and Haddon R C 1992 *Nature* **355** 529
[21] Kortan A R, Kopylov N, Özdas E, Ramirez A P, Fleming R M and Haddon R C 1994 *Chem. Phys. Lett.* **223** 501
[22] Kortan A R, Kopylov N, Glarum S, Gyorgy E M, Ramirez A P, Fleming R M, Zhou O, Thiel F A, Trevor P L and Haddon R C 1992 *Nature* **360** 566

[23] Baenitz M, Heinze M, Lüders K, Werner H, Schlögl R, Weiden M, Sparn G and Steglich F 1995 *Solid State Commun.* **96** 539
[24] Brown C M, Taga S, Gogia B, Kordatos K, Margadonna S, Prassides K, Iwasa Y, Tanigaki K, Fitch A N and Pattison P 1999 *Phys. Rev. Lett.* **83** 2258
[25] Iwasa Y, Hayashi H, Furudate T and Mitani T 1996 *Phys. Rev.* B **54** 14960
[26] Iwasa Y, Kawaguchi M, Iwasaki H, Mitani T, Wada T and Hasegawa T 1998 *Phys. Rev.* B **57** 13395
[27] Özdas E, Kortan A R, Kopylov N, Ramirez A P, Siegrist T, Rabe K M, Bair S, Schuppler S and Citrin P H 1995 *Nature* **375** 126
[28] Chen X H and Roth G 1995 *Phys. Rev.* B **52** 15534
[29] Chen X H, Taga S and Iwasa Y 1999 *Phys. Rev.* B **60** 4351
[30] Citrin P H, Özdas E, Schuppler S, Kortan A R and Lyons K B 1997 *Phys. Rev.* B **56** 5213
[31] Prassides K 1997 *Curr. Opin. Solid State Mater. Sci.* **2** 433
[32] Rosseinsky M J 1998 *Chem. Mater.* **10** 2665
[33] Gunnarsson O 1997 *Rev. Mod. Phys.* **69** 575
[34] Yildirim T, Zhou O and Fischer J E 2000 *The Physics of Fullerene-Based and Fullerene-Related Materials* ed W Andreoni (Dordrecht: Kluwer–Academic) p 23
[35] Dahlke P, Denning M S, Henry P F and Rosseinsky M J 2000 *J. Am. Chem. Soc.* **122** 12352
[36] Lof R W, van Veenendaal M A, Koopmans B, Jonkman H T and Sawatzky G A 1992 *Phys. Rev. Lett.* **68** 3942
[37] Chauvet O, Oszlanyi G, Forro L, Stephens P W, Tegze M, Faigel G and Janossy A 1994 *Phys. Rev. Lett.* **72** 2721
[38] Iwasa Y, Shimoda H, Palstra T T M, Maniwa Y, Zhou O and Mitani T 1996 *Phys. Rev.* B **53** R8836
[39] Allen K M, Heyes S J and Rosseinsky M J 1996 *J. Mater. Chem.* **6** 3956
[40] Prassides K, Margadonna S, Arcon D, Lappas A, Shimoda H and Iwasa Y 1999 *J. Am. Chem. Soc.* **121** 11227
[41] Simon F, Janossy A, Muranyi F, Feher T, Shimoda H, Iwasa Y and Forro L 2000 *Phys. Rev.* B **61** R3826
[42] Tou H, Maniwa Y, Iwasa Y, Shimoda H and Mitani T 2000 *Phys. Rev.* B **62** R775
[43] Fleming R, Rosseinsky M J, Ramirez A P, Murphy D W, Tully J C, Haddon R C, Siegrist T, Tycko R, Glarum S H, Marsh P, Dabbagh G, Zahurak S M, Makhija A V and Hampton C 1991 *Nature* **352** 701
[44] Dahlke P, Henry P F and Rosseinsky M J 1998 *J. Mater. Chem.* **8** 1571
[45] Eklund P C, Zhou O, Wang K-A, Dresselhaus G and Dresselhaus M S 1992 *J. Phys. Chem. Solids* **53** 1391
[46] Umemoto K, Saito S and Oshiyama A 1999 *Phys. Rev.* B **60** 16186
[47] Margadonna S, Aslanis E, Li W Z, Prassides K, Fitch A N and Hansen T C 2000 *Chem. Mater.* **12** 2736
[48] Murphy D W, Rosseinsky M J, Fleming R M, Tycko R, Ramirez A P, Haddon R C, Siegrist T, Dabbagh G, Tully J C and Walstedt R E 1992 *J. Phys. Chem. Solids* **53** 1321
[49] Kiefl R F, Duty T L, Schneider J W, MacFarlane A, Chow K, Elzey J W, Mendels P, Morris G D, Brewer J H, Ansaldo E J, Niedermayer C, Noakes D R, Stronach C E, Hitti B and Fischer J E 1992 *Phys. Rev. Lett.* **69** 2005
[50] Iwasa Y and Kaneyasu T 1995 *Phys. Rev.* B **51** 3678
[51] Erwin S C 1992 *Buckminsterfullerenes* ed W E Billups and M A Ciufolini (New York: VCH)
[52] Yildirim T, Fischer J E, Harris A B, Stephens P W, Liu D, Brard L, Strongin R M and Smith A B III 1993 *Phys. Rev. Lett.* **71** 1383
[53] Kubozono Y *et al* 1999 *Phys. Rev.* B **59** 15062
[54] Brouet V, Alloul H, Le T-N, Garaj S and Forro L 2001 *Phys. Rev. Lett.* **86** 4680
[55] Himmel K and Jansen M 1998 *Inorg. Chem.* **37** 3437
[56] Bhyrappa P, Paul P, Stinchcombe J, Boyd P D W and Reed C A 2000 *J. Am. Chem. Soc.* **115** 11004
[57] Knupfer M and Fink J 1997 *Phys. Rev. Lett.* **79** 2714
[58] Dahlke P and Rosseinsky M J 2002 *Chem. Mater.* **14** 1285
[59] Umemoto K and Saito S 2000 *Phys. Rev.* B **61** 14204
[60] Saito S and Oshiyama A 1993 *Phys. Rev. Lett.* **71** 121
[61] Erwin S C and Pederson M R 1993 *Phys. Rev.* B **47** 14657
[62] Takenobu T, Muro T, Iwasa Y and Mitani T 2000 *Phys. Rev. Lett.* **85** 381
[63] Manini N and Tosatti E 2002 *Phys. Rev.* B **66** 115107
[64] Kitano H, Matsuo R, Miwa K, Maeda A, Takenobu T, Iwasa Y and Mitani T 2002 *Phys. Rev. Lett.* **88** 096401
[65] Lu J P 1994 *Phys. Rev.* B **49** 5687
[66] Gunnarsson O, Koch E and Martin R M 1996 *Phys. Rev.* B **54** R11026
[67] Chida T, Suzuki S and Nakao K 2001 *J. Phys. Soc. Japan* **70** 317
[68] Fischer J E and Heiney P A 1993 *J. Phys. Chem. Solids* **54** 1725
[69] Dresselhaus M S, Dresselhaus G and Eklund P C 1996 *Science of Fullerenes and Carbon Nanotubes* (San Diego, CA: Academic)

[70] Yoshinari Y, Alloul H, Kriza G and Holczer K 1993 *Phys. Rev. Lett.* **71** 2413
[71] Ishii K, Watanuki T, Fujiwara A, Suematsu H, Iwasa Y, Shimoda H, Mitani T, Nakao H, Fujii Y, Murakami Y and Kawada H 1999 *Phys. Rev.* B **59** 3956
[72] Margadonna S, Prassides K, Shimoda H, Takenobu T and Iwasa Y 2001 *Phys. Rev.* B **64** 132414
[73] Kugel K I and Khomskii D I 1982 *Sov. Phys.–Usp.* **25** 231 and references therein
For recent advances, see
Tokura Y and Nagaosa N 2000 *Science* **288** 462
[74] Allemand P-M, Khemani K C, Koch A, Wudl F, Holczer K, Donovan S, Gruner G and Thompson J D 1991 *Science* **253** 301
[75] For example
Kinoshita M 1989 *Mol. Cryst. Liq. Cryst.* **176** 163
[76] Kawamoto T, Tokumoto M, Sakamoto H and Mizoguchi K 2001 *J. Phys. Soc. Japan* **70** 1892
[77] Mizoguchi K, Machino M, Sakamoto H, Kawamoto T, Tokumoto M, Omerzu A and Mihailovic D 2001 *Phys. Rev.* B **63** 140417
[78] Narymbetov B, Omerzu A, Kavanov V V, Tokumoto M, Kobayashi H and Mihailovic D 2001 *Nature* **407** 883
[79] Suzuki S, Okada S and Nakao K 2000 *J. Phys. Soc. Japan* **69** 2615